

# Negatively charged Si vacancy in 4H SiC: A comparison between theory and experiment

T. Wimbauer

*Walter Schottky Institut, Technische Universität München, Am Coulombwall, D-85748 Garching, Germany*

B. K. Meyer, A. Hofstaetter, and A. Scharmann

*I. Physikalisches Institut, Justus-Liebig-Universität Gießen, Heinrich Buff Ring 16, D-35392 Gießen, Germany*

H. Overhof

*Fachbereich Physik, Universität-GH Paderborn, Warburgerstraße 100 A, D-33098 Paderborn, Germany*

(Received 25 March 1997)

We use electron paramagnetic resonance and electron nuclear double resonance to identify the negatively charged Si vacancy in neutron-irradiated 4H SiC. The identification is based on resolved ligand hyperfine interactions with carbon and silicon nearest and next nearest neighbors and on the determination of the spin state, which is  $S=3/2$ . The magnetic resonance parameters of  $V_{Si}^-$  are almost identical for the polytypes 3C, 4H, and 6H. The experimental findings are supported by theoretical ligand hyperfine interaction data based on a total-energy calculation using the standard local-density approximation of the density-functional theory. [S0163-1829(97)06635-6]

## I. INTRODUCTION

Lattice vacancies can conveniently be created in semiconductors by electron or neutron irradiation.<sup>1,2</sup> They usually introduce energy levels in the gap, and can, therefore, exist in different charge states and act as efficient recombination centers.<sup>1</sup> Most vacancies are thermally quite stable. In the case of SiC, vacancies do not anneal out below 750 °C.<sup>3</sup>

The electronic structure of vacancies is understood within a one-electron orbital model.<sup>1</sup> The removal of a lattice atom introduces four dangling-bonds at the four ligands next to the vacancy thus created. For an undistorted vacancy in a cubic crystal, these dangling-bond orbitals are to be symmetrized and, therefore, transform according to the  $a_1$  and  $t_2$  irreducible representations of the group  $T_d$ , respectively. In Si, diamond, and also in GaP the state transforming according to  $a_1$  forms a resonance in the valence band. Hence, it is occupied and plays no role in the electrical activity of the vacancy.

In contrast, the state that transforms according to  $t_2$  gives rise to a gap state. For the case of the neutral Ga vacancy in GaP and also the negatively charged vacancies in diamond and in silicon, this state is occupied by three electrons. For this occupation two distinct electronic ground states are possible. If the spin-spin interaction is larger than the spin-lattice interaction, a spin  $S=3/2$  high-spin state forms the ground state of the system. This state is a  $^4A_2$  spin quartet state, which is an orbital singlet and not subject to a Jahn-Teller distortion. From ENDOR investigations and EPR experiments under applied uniaxial stress it is known that this is the case for the Ga vacancy in GaP (Refs. 4 and 5) and for the vacancy in diamond.<sup>2</sup> For the negatively charged vacancy in silicon, however, the other possible state, the low-spin  $S=1/2$  state is found to be the ground state. The low-spin ground state of the undistorted vacancy would be an orbital multiplet which, however, undergoes a static Jahn-Teller distortion and thereby gives rise to a spin  $S=1/2$  orbital singlet state that has tetragonal symmetry.

In the 3C, 4H, and 6H polytypes of SiC vacancies are also introduced by particle irradiation. One of the defects introduced by particle irradiation has tentatively been assigned to the negatively charged Si vacancy in a recent report.<sup>6</sup> The EPR spectra of this defect are characterized by an isotropic  $g$  factor that can be interpreted in two alternative ways: (i) we observe a high-spin  $S=3/2$  orbital singlet state  $^4A_2$  with negligible fine-structure splitting or (ii) the ground state is a low-spin state and a dynamical Jahn-Teller effect leads to the perfect isotropy of the  $g$  factor. In this paper we shall resolve this ambiguity by ENDOR experiments that prove that we have a high-spin ground state for the Si vacancy in 4H SiC. Since EPR results for 3C SiC and 6H SiC (Refs. 7 and 8) are very similar to the results presented here for 4H SiC, we conclude that all three polytypes of SiC have a similar high-spin orbital ground state.

We have also calculated ligand hyperfine interactions for the nearest- and next-nearest-neighbor shell of the Si vacancy in 3C SiC based on *ab initio* calculations. We find a very close agreement of the calculated isotropic and anisotropic hyperfine interactions with the experimental ENDOR data, which provides a further confirmation of our defect assignment.

## II. DETAILS OF THE INVESTIGATION

### A. Experiment

An X-band EPR spectrometer (Bruker ER 420-SP) with a TE<sub>102</sub> rectangular cavity, 100 kHz modulation, and lock-in detection was used; the derivative of the absorption was thus obtained. The microwave frequency was measured with an electronic counter and the magnetic field with a proton resonance probe. In this way  $g$  values accurate to  $\pm 0.0001$  could be obtained. ENDOR measurements were done on a Bruker ESP 300 E spectrometer with a TM<sub>110</sub> cavity including the ENDOR coil and frequency modulation of the radio frequency.

The investigated 4H SiC sample was irradiated with reactor neutrons. The radiation fluence (dose) was  $\Phi_n = 10^{16} \text{ cm}^{-2}$ .

### B. Theory

We have performed *ab initio* total-energy calculations using the standard local-spin-density approximation<sup>9–11</sup> of the density-functional theory<sup>12,13</sup> (DFT-LSDA) to determine the electronic ground-state properties of the vacancy. The computational scheme has been discussed in detail in a theoretical paper<sup>14</sup> as well as in several applications.<sup>15,16</sup> We therefore can restrict the presentation of the theoretical method to a few essential points.

We solve the problem of a deep defect in a crystal using a Green's-function technique. We start with a band-structure calculation using the linear-muffin-tin-orbitals method in the atomic-spheres approximation (LMTO-ASA) in order to determine the Green's function  $G^0$  of the unperturbed crystal. Next we solve a Dyson equation for  $G(\mathbf{r}, \mathbf{r}', E)$ :

$$G(\mathbf{r}, \mathbf{r}', E) = G^0(\mathbf{r}, \mathbf{r}', E) + \int G^0(\mathbf{r}, \mathbf{r}'', E) \Delta V(\mathbf{r}'') G(\mathbf{r}'', \mathbf{r}', E) d^3 \mathbf{r}'', \quad (1)$$

where  $\Delta V = V - V^0$  is the difference between the one-particle potentials of the crystal containing the impurity and that of the unperturbed crystal. Since for deep impurities  $\Delta V$  may have large values, which, however, are restricted to a small spatial region around the impurity, we divide the crystal into a ‘‘perturbed region’’ (containing the atomic spheres of the impurity atom, of a few neighboring host atoms and of space-filling interstitial spheres) and into the ‘‘unperturbed’’ crystal outside this region. Our perturbed region for the vacancy consists of the Si atomic host sphere for the vacancy and of 12 atomic spheres that contain the silicon next-nearest neighbors, of four spheres that contain the nearest-neighbor carbon atoms, and of 10 interstitial spheres. Within the perturbed region Dyson's equation is solved self-consistently, outside this region  $G$  is approximated by  $G^0$ .

In our approach the total energy of the crystal containing a vacancy must be calculated ignoring lattice

relaxations.<sup>14–16</sup> We calculate the change in total energy introduced by the vacancy. To this quantity we add the energy of the long-range Coulomb part of  $n \times 0.1 \text{ eV}$ , where  $n$  indicates the charge state of the impurity.<sup>15,17</sup> In order to compare total energies for different charge states of a defect we discuss the  $n$ -times charged defect  $V^{(n)}$  plus  $n$  electrons or holes that are transferred to the Fermi level. Thus the total energy becomes a function of the Fermi level  $E_F$ :

$$E_{\text{tot}}(V^{(n)}, E_F) = E_{\text{tot}}^b(V^{(n)}) + nE_F, \quad (2)$$

where  $E_{\text{tot}}^b$  is the energy of the vacancy for a Fermi level at the valence-band edge. With these total energies we calculate the electron removal energies, which are those positions of the Fermi level for which the total energies of the two charge states coincide.

The computation of the hyperfine interactions (hfi) for  $V_{\text{Si}}^-$  is relatively simple, because we can deal with an  $S=3/2$  orbital singlet state as shown below. In this case we have no contributions from the orbital momentum. The isotropic hyperfine interaction for an electron state with  $g$  factor  $g_e$  interacting with a nucleus with  $g$  factor  $g_N$  at the site  $\mathbf{R}_N$  is given by

$$a_N = \frac{2}{3} \frac{1}{2S} \mu_0 g_e g_N \mu_N m(\mathbf{R}_N), \quad (3)$$

where  $\mu_0$  is the susceptibility constant and  $\mu_N$  is the nuclear magneton. The magnetization density  $m(\mathbf{R}_N)$  at the nuclear site  $\mathbf{R}_N$  is the product of Bohr's magneton  $\mu_B$  and the difference  $m(\mathbf{r})$  between the electron spin densities of up and down spins  $n_\uparrow$  and  $n_\downarrow$ , respectively,

$$m(\mathbf{r}) = \mu_B [n_\uparrow(\mathbf{r}) - n_\downarrow(\mathbf{r})]. \quad (4)$$

The anisotropic (dipolar) hfi is given by an integral over the magnetization density over all space,

$$(b_N)_{i,j} = \frac{\mu_0}{8\pi} \frac{1}{2S} g_e g_N \mu_N \int \frac{3x_i x_j - r^2 \delta_{i,j}}{r^5} m(\mathbf{r} + \mathbf{R}_N) d\mathbf{r}. \quad (5)$$

The integrand is strongly peaked at the nucleus and, therefore, it is sufficient to perform the integration over the central ASA sphere. The contributions from the other spheres can be

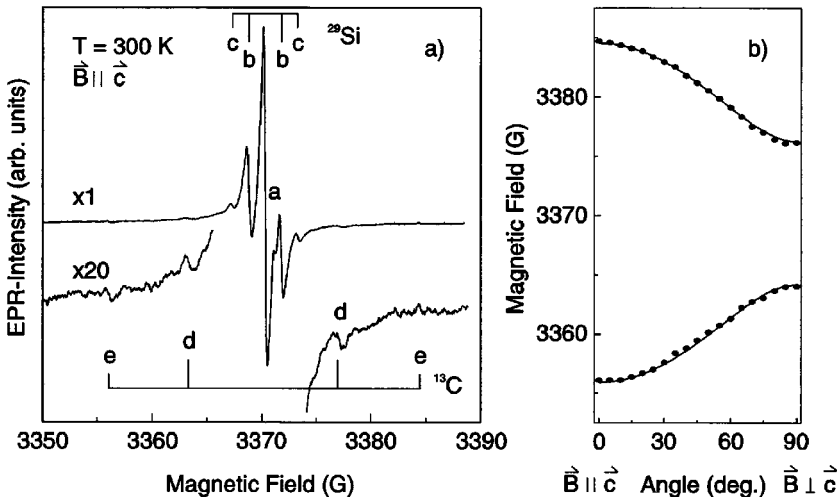


FIG. 1. (a) EPR spectrum of the isolated Si vacancy in 4H SiC. The satellite lines are caused by hyperfine interaction with nearest-neighbor  $^{13}\text{C}$  and next-nearest-neighbor  $^{29}\text{Si}$  ligands. (b) Angular dependence for the hyperfine interaction with the axial  $^{13}\text{C}$  ligands of the Si vacancy. The solid lines correspond to a fit of the experimental data (see text for details).

TABLE I. Experimental  $g$  values and parameters for the hyperfine structure of the Si vacancy in  $3C$ ,  $4H$ , and  $6H$  SiC.

	$g$	$A_{\text{Si}}$ (G)	$A_{\text{C}\parallel}$ (G)	$A_{\text{C}\perp}$ (G)
$4H$ SiC	2.0034	2.98	28.6	12.1
$6H$ SiC	2.0015	2.97	28.7	11.5
$3C$ SiC	2.0029	2.94	26.6	11.8

approximated replacing the spin distribution in each of these spheres by point dipoles with a dipole moment appropriate for the integrated spin density in the spheres.

### III. RESULTS AND DISCUSSION

Figure 1(a) shows the EPR spectrum of the  $4H$  SiC sample for  $\mathbf{B}\parallel\mathbf{c}$  orientation, measured at room temperature. The EPR spectrum is described by the following spin Hamiltonian:

$$H = \mu_B \mathbf{S} \tilde{g} \mathbf{B} + \sum_{i=1}^4 \mathbf{S} \tilde{A}_C \mathbf{I}_C + \sum_{i=1}^4 g_{N,C} \mu_N \mathbf{B} \mathbf{I}_C + \sum_{i=1}^{12} \mathbf{S} \tilde{A}_{\text{Si}} \mathbf{I}_{\text{Si}} + \sum_{i=1}^{12} g_{N,\text{Si}} \mu_N \mathbf{B} \mathbf{I}_{\text{Si}}, \quad (6)$$

in which the symbols have their usual meanings. The interaction parameters are listed in Table I. For comparison, the parameters for the Si vacancy in  $3C$  SiC (Ref. 7) and  $6H$  SiC (Ref. 8) are also listed. The central line (line  $a$ ) of the EPR spectrum is the Zeeman line ( $I=0$ ), while the satellite lines (lines  $b$ ,  $c$ ,  $d$ , and  $e$ ) arise from hyperfine interactions with the nearest and the next-nearest neighbors with nonzero nuclear spin, i.e.,  $^{13}\text{C}$  (nuclear spin  $I_C=1/2$ ; natural abundance 1.1%) and  $^{29}\text{Si}$  (nuclear spin  $I_{\text{Si}}=1/2$ ; natural abundance 4.7%). All configurations with one  $^{29}\text{Si}$  atom in the next-nearest-neighbor shell of the Si vacancy contribute to the lines  $b$ ; configurations with two  $^{29}\text{Si}$  atoms in the next-nearest-neighbor shell contribute to the lines  $c$ . For these Si superhyperfine lines no anisotropy was detectable. In contrast, lines  $d$  and  $e$ , which originate from one  $^{13}\text{C}$  atom in the nearest-neighbor shell are anisotropic. Among the nearest C neighbors one distinguishes between axial ligands (direction of the bond along the  $c$  axis) and basal ligands (the angle between the direction of the bond and  $c$  axis is a tetraeder angle). For  $\mathbf{B}\parallel\mathbf{c}$ , we observe two lines for axial (lines  $d$ ) and basal (lines  $e$ ) ligands. The angular dependence of the axial ligands is shown in Fig. 1(b).

TABLE II. Calculated and measured relative intensities of  $^{13}\text{C}$  and  $^{29}\text{Si}$  ligand hyperfine lines.

Intensity ratio	Theory	Experiment
$b/a$	0.265	0.256
$c/a$	0.036	0.026
$d/a$	0.005	0.002
$e/a$	0.015	0.004

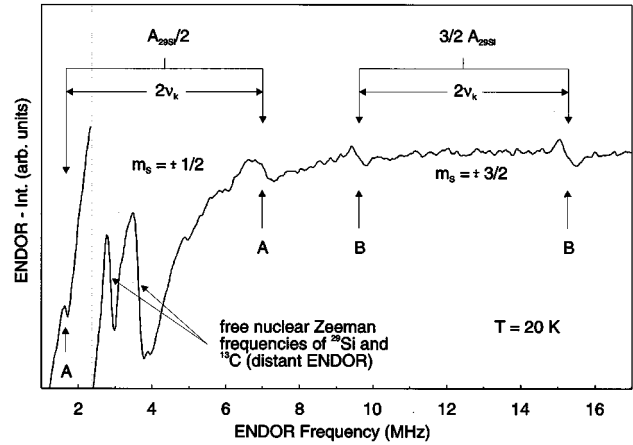


FIG. 2. ENDOR spectrum detected on the low-field Si hyperfine line labeled  $b$  in (b). The lines labeled  $B$  are connected with the  $m_S = \pm 3/2$  and the lines labeled  $A$  with the  $m_S = \pm 1/2$  spin states. Between 2 and 4 MHz the distant ENDOR lines of C and Si nuclei are seen.

Using the natural abundances of  $^{13}\text{C}$  and  $^{29}\text{Si}$  one calculates for the probability that one of the  $^{13}\text{C}$  atoms is among the four nearest neighbors a value of 0.043; the probability for one  $^{29}\text{Si}$  atom among the 12 next-nearest neighbors is 0.331 and for two  $^{29}\text{Si}$  atoms 0.089. Thus we expect the intensity ratios shown in Table II. We see that the experimental ratios are in good agreement with the values deduced from the natural abundances.

In a simple first order solution of the spin Hamiltonian (6), the frequency of an ENDOR line  $\nu$  ignoring the C hyperfine interaction is given by

$$\nu = \frac{1}{h} |m_S A_{\text{Si}} - g_{N,\text{Si}} \mu_N B_0| = \frac{1}{h} |m_S A_{\text{Si}} - \nu_k|. \quad (7)$$

The second term in Eq. (7) is the free nuclear frequency  $\nu_k$ . Equation (7) immediately explains why ENDOR can be used to determine the spin state of the defect. In the case of  $S = 1/2$  one expects two transitions according to the  $m_S = \pm 1/2$  doublet. For spin  $S = 3/2$  four transitions are expected, the  $m_S = \pm 3/2$  doublet and the  $m_S = \pm 1/2$  doublet. An experimental spectrum, detected at 20 K on the low-field Si hyperfine line labeled  $b$  in Fig. 1(a), is shown in Fig. 2. At 2.98 MHz and 3.75 MHz the distant ENDOR lines of  $^{29}\text{Si}$  and  $^{13}\text{C}$  are seen (free nuclear frequency of  $^{29}\text{Si}$  and  $^{13}\text{C}$ ). The four lines at 1.6 MHz, 7.11 MHz, 9.52 MHz, and 15.19 MHz arise from the interaction with  $^{29}\text{Si}$ . Lines  $B$  are connected with the  $m_S = \pm 3/2$  and lines  $A$  with the  $m_S = \pm 1/2$  spin states. Within every  $m_S$  doublet the lines are separated by approximately twice the free nuclear frequency of  $^{29}\text{Si}$  ( $2\nu_k = 5.71$  MHz). For  $m_S = \pm 3/2$  we obtain  $A_{\text{Si}} = 8.24$  MHz ( $A_{\text{Si}} = 2.94$  G) and for  $m_S = \pm 1/2$  we get  $A_{\text{Si}} = 8.71$  MHz ( $A_{\text{Si}} = 3.11$  G). These values agree within the experimental accuracy with the hyperfine constant  $A_{\text{Si}} = 2.98$  G obtained from the EPR analysis.

Our theoretical hyperfine interactions have been obtained for the unrelaxed vacancy in  $3C$  SiC only. From an inspection of the experimentally determined hfi data in Table I we see that in the case of the high-spin state the hfi for the  $V_{\text{Si}}^-$

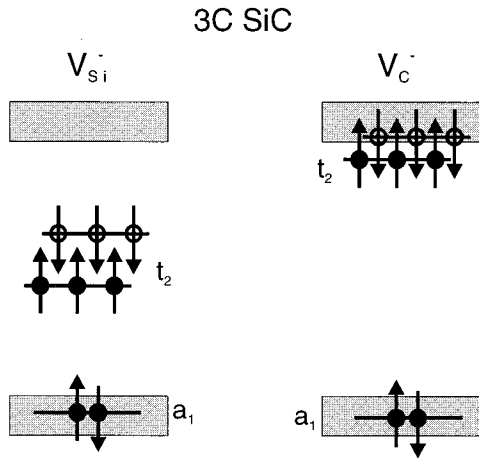


FIG. 3. Single-particle energies for the unrelaxed vacancies  $V_{\text{Si}}^-$  and  $V_{\text{C}}^-$  in 3C SiC in the high-spin negative charge state. The arrows indicate the spin-up and spin-down states; full circles stand for occupied and empty circles for unoccupied single-particle states, respectively.

defects in 6H and 4H SiC are hardly different from those in 3C SiC. Furthermore, the different inequivalent  $V_{\text{Si}}^-$  lattice sites lead to Zeeman and hfi splittings that are too small to be resolved experimentally. We have therefore avoided the extensive computational effort connected with the calculation for the hexagonal polytypes. As stated above the use of the ASA prevents the inclusion of lattice relaxations. This appears to be no serious limitation when calculating electronic properties like hfi interactions for orbital singlet states.

In Fig. 3 the single-particle energies of the negatively charged vacancies in the high-spin state are shown. The single-particle states that transform according to the  $a_1$  irreducible representation are resonances just below the valence-band edge, whereas the  $t_2$  dangling bondlike states are located in the center of the band gap. For the isoelectronic  $V_{\text{C}}^-$  defect in 3C SiC the dangling-bond states are very close to the conduction-band edges but also very localized. We show in Fig. 4 a contour plot in the (110) plane of the total spin density of  $V_{\text{Si}}^-$ . Most of the spin density originates from localized gap states with minor contributions only from the polarization of the valence bands and even less from the spin polarization of the inner (core) shells of the ligands.

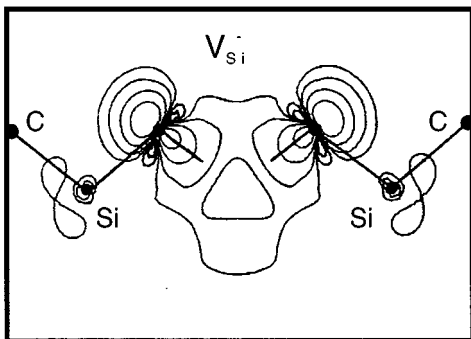


FIG. 4. Contour plot of the total spin-density distribution for the negatively charged  $V_{\text{Si}}^-$  in the (110) plane. The C(1,1,1) and Si(2,2,0) nuclei are indicated by full dots.

TABLE III. Theoretical and experimental values of 3C SiC for the splitted hyperfine parameters  $A$  into isotropic and dipolar contributions ( $a$  and  $b$ , respectively) of the corresponding wave functions according to  $A_{\parallel} = a + 2b$  and  $A_{\perp} = a - b$ .

	Theory	Experiment
$a_{\text{Si}}$ (G)	2.56	$\pm 2.94$
$b_{\text{Si}}$ (G)	-0.0013	0
$a_{\text{C}}$ (G)	25.5	16.7
$b_{\text{C}}$ (G)	4.2	4.9

A comparison with the same charge state of the vacancy in crystalline silicon shows that the particle density at the next-nearest ligands (of the dangling-bond states) for  $V_{\text{Si}}^-$  in 3C SiC is about three times more localized than in Si. As a consequence, the exchange splitting between the spin-up and spin-down states that transform according to  $t_2$  in 3C SiC is by about the same factor of three larger than in the case of Si.

Unfortunately, the use of the ASA prevents us from studying in detail the most interesting question; why in SiC the  $V_{\text{Si}}^-$  is stable in a high-spin configuration whereas the isoelectronic  $V_{\text{Si}}^-$  vacancy in Si is not stable in a spin 3/2 state. It is obvious that the larger energy separation of the two spin configurations in SiC (0.38 eV for  $V_{\text{Si}}^-$  in 3C SiC, as compared to 0.13 eV for  $V^-$  in Si) tends to stabilize the high-spin configuration. The Jahn-Teller energies reported for the  $V^-$  defect in Si,<sup>1</sup> however, would be larger than 0.38 eV.

The calculated hyperfine interactions listed in Table III compare well with their experimental counterparts. For the hfi with the  $^{13}\text{C}(1,1,1)$  nearest-neighbor nuclei we observe that the calculated contact term is somewhat too large (as compared to the experimental value) whereas the dipolar term turns out to be somewhat too small. This could be indicative of a breathing distortion around the vacancy, the

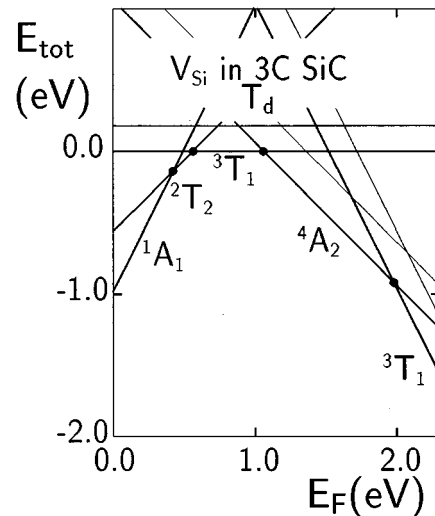


FIG. 5. Total energies  $E_{\text{tot}}(E_F)$  for the unrelaxed vacancy  $V_{\text{Si}}^{(n)}$  in the charge state  $n$ . Full lines are for the high-spin and thin lines for the low-spin configurations, respectively. Full circles mark electron removal energies.

only lattice relaxation expected for an  ${}^4A_2$  state. The contact hfi with the  ${}^{29}\text{Si}(2,2,0)$  next-nearest-neighbor nuclei has a positive sign according to our calculation, i.e., corresponds to a negative spin density (as the nuclear  $g$  factor  $g_N$  is negative for  ${}^{29}\text{Si}$ ).

It should be noted that the agreement of the experimental with the calculated hfi data does not for itself provide evidence that the negative charge state of the vacancy has  $S = 3/2$ : a calculation for a  $S = 1/2$  state ignoring Jahn-Teller distortions (which for this orbitally degenerate state must be present but might be small) leads to practically identical hfi constants as might be expected.

Finally, the total energies  $E_{\text{tot}}(V^{(n)}, E_F)$  are shown in Fig. 5 for the high-spin configurations (full lines) and for low-spin configurations (thin lines), respectively. In the absence of Jahn-Teller effect the high-spin states are trivially lower in energy than the low-spin states. We calculate transition (ionization) energies of  $E^{+/+/+} = 0.42$  eV,  $E^{+/0} = 0.54$  eV,  $E^{0/-} = 1.06$  eV, and  $E^{-/-} = 1.96$  eV, respectively, for the unrelaxed vacancies.

#### IV. CONCLUSIONS

We observed the Si vacancy in  $4H$  SiC in its singly negatively charge state by EPR after neutron irradiation of the sample. The interaction parameters are hardly different from those in the polytypes  $3C$  and  $6H$  as seen in Table I. The EPR spectrum is isotropic as well as the ligand hyperfine interactions with next-nearest Si nuclei are isotropic. This immediately raised the question whether  $V_{\text{Si}}^-$  in SiC has a high-spin configuration ( $S = 3/2$ ) or whether a strong Jahn-Teller-Effect leads to an isotropic EPR signal for  $S = 1/2$ . Based on ENDOR experiments we find unambiguously the spin state of  $V_{\text{Si}}^-$  in  $4H$  SiC to be  $S = 3/2$ .

Using the spin-density approximation of the density-functional theory the ground-state properties of the Si vacancy were determined to support the experimental findings. Within this theoretical formalism, total energies, the spin density distribution, and the hyperfine constants of the Si vacancy were obtained, which are in good agreement with the experiment.

- 
- <sup>1</sup>G. Watkins, in *Deep Centers in Semiconductors*, edited by S. T. Pantelides (Gordon and Breach, New York, 1986), p. 147.
- <sup>2</sup>J. Isoya, H. Kanda, Y. Uchida, S. C. Lawson, S. Yamasaki, H. Itoh, and Y. Morita, *Phys. Rev. B* **45**, 1436 (1992).
- <sup>3</sup>H. Itoh, N. Hayakawa, I. Nashiyama, and E. Sakuma, *J. Appl. Phys.* **66**, 4529 (1989).
- <sup>4</sup>T. A. Kennedy, N. D. Wilsey, J. J. Krebs, and G. H. Stauss, *Phys. Rev. Lett.* **50**, 1281 (1983).
- <sup>5</sup>J. Hage, J. R. Niklas, and J.-M. Spaeth, in *Proceedings of the 14th International Conference on Defects in Semiconductors*, edited by H. F. von Bardeleben [*Mater. Sci. Forum* **10-12**, 259 (1986)].
- <sup>6</sup>T. Wimbauer, D. Volm, B. K. Meyer, A. Hofstaetter, and A. Scharmann, in *Proceedings of the 23rd International Conference on Physics of Semiconductors*, edited by M. Scheffler and R. Zimmermann (World Scientific, Singapore, 1996), p. 2649.
- <sup>7</sup>H. Itoh, M. Yoshikawa, I. Nashiyama, S. Misawa, H. Okumura, and S. Yoshida, *IEEE Trans. Nucl. Sci.* **37**, 1732 (1990).
- <sup>8</sup>J. Schneider and K. Maier, *Physica B* **185**, 199 (1993).
- <sup>9</sup>U. von Barth and L. Hedin, *J. Phys. C* **5**, 1629 (1972).
- <sup>10</sup>D. Ceperley, *Phys. Rev. B* **18**, 3126 (1978).
- <sup>11</sup>D. M. Ceperley and B. J. Alder, *Phys. Rev. Lett.* **45**, 566 (1980).
- <sup>12</sup>P. Hohenberg and W. Kohn, *Phys. Rev.* **136**, B864 (1964).
- <sup>13</sup>W. Kohn and L. J. Sham, *Phys. Rev.* **140**, A1133 (1965).
- <sup>14</sup>O. Gunnarsson, O. Jepsen, and O. K. Andersen, *Phys. Rev. B* **27**, 7144 (1993).
- <sup>15</sup>F. Beeler, O. K. Andersen, and M. Scheffler, *Phys. Rev. Lett.* **55**, 1498 (1985); *Phys. Rev. B* **41**, 1603 (1990).
- <sup>16</sup>F. Beeler and M. Scheffler, in *Proceedings of the 15th International Conference of Defects in Semiconductors*, edited by G. Ferenczi [*Mater. Sci. Forum* **38-41**, 257 (1989)].
- <sup>17</sup>C. O. Rodriguez, S. Brand, and M. Jaros, *J. Chem. Phys.* **13**, L333 (1980).